Acta Crystallographica Section D
Biological Crystallography
ISSN 0907-4449

Structure of the cytosolic Cu,Zn superoxide dismutase from *Schistosoma mansoni*

Rosa M. F. Cardoso,[a,b] Carlos H. T. P. Silva,[a]‡ Ana Paula Ulian de Araújo,[a] Tomoo Tanaka,[c] Manami Tanaka[c,d] and Richard C. Garratt[a]*

[a]Instituto de Física de São Carlos, Universidade de São Paulo, Av. Trabalhador Sãocarlense 400, São Carlos, SP, 13566-590, Brazil, [b]Instituto de Química de São Carlos, Universidade de São Paulo, Av. Trabalhador Sãocarlense 400, São Carlos, SP, 13566-590, Brazil, [c]Tokai University School of Medicine, Isehara, Kanagawa 259-1193, Japan, and [d]National Institute of Advanced Industrial Science and Technology, Tsukuba Central 6-1-421, Higashi, Tsukuba Science City, Ibaraki 305-8566, Japan

‡ Current address: Faculdade de Ciências Farmacêuticas de Ribeirão Preto, Universidade de São Paulo, Av. do Café, s/n, Ribeirão Preto, SP, 14040-903, Brazil.

Correspondence e-mail: richard@if.sc.usp.br

Received 15 April 2004
Accepted 8 July 2004

PDB References: Cu,Zn superoxide dismutase, 1to4, r1to4sf; 1to5, r1to5sf.

Cu,Zn superoxide dismutase (Cu,Zn SOD) is an essential enzyme for protecting cells from the toxic effects of reactive oxygen species. In humans, two distinct Cu,Zn SOD genes are located on chromosomes 4 and 21 and mutations in the latter have been associated with familial amyotrophic lateral sclerosis. Similarly, schistosomes (trematode parasites responsible for the chronically debilitating disease schistosomiasis) also produce two distinct Cu,Zn SODs, in this case one cytosolic and one bearing a signal peptide. The crystal structure of the cytosolic form of the enzyme from the human trematode *Schistosoma mansoni* (SmCtSOD) was solved and refined to a resolution of 2.2 Å (space group $P2_12_12_1$, $R = 17.6\%$ and $R_{\rm free} = 24.1\%$) and 1.55 Å (space group $P2_1$, $R = 15.7\%$ and $R_{\rm free} = 17.1\%$). This is the first report of a crystal structure of a Cu,Zn superoxide dismutase derived from a human parasite. Alternate positions for the catalytic copper and its water ligand were refined for the 1.55 Å SmCtSOD model, but the most interesting structural differences between SmCtSOD and the human homologue reside in the loops used for electrostatic guidance of the substrate to the enzyme active site.

1. Introduction

Cu,Zn superoxide dismutase (SOD), an essential enzyme for protecting cells from the toxic products of aerobic metabolism, catalyzes the disproportionation of the superoxide radical to hydrogen peroxide and oxygen by alternately oxidizing and reducing the copper (Fridovich, 1986; Tainer *et al.*, 1990; Winterbourn, 1993). Many free radicals are scavenged by dioxygen to form superoxide (Winterbourn, 1993) and SOD, which removes the superoxide, is therefore a master regulator of free-radical balance and reactive oxygen species in cells (Winterbourn, 1993).

Cytosolic Cu,Zn SOD assembles into an unusually stable homodimer with exquisite substrate specificity. This enzyme uses electrostatic attraction to achieve faster than diffusion substrate recognition (Richardson, 1981; Tainer *et al.*, 1990). The turnover rate of the enzyme is rapid because the enzyme couples efficient alterations in copper-site geometry with catalysis. The independent evolution of the dimer interface and the electrostatic elements in eukaryotes and prokaryotes indicate that these are important features of Cu,Zn SOD (Bourne *et al.*, 1996; Forest *et al.*, 2000).

Three-dimensional structures are known in detail for Cu,Zn SODs from various species, including ox (Tainer *et al.*, 1982), spinach (Kitagawa *et al.*, 1991), yeast (Djinovic *et al.*, 1992), human (Parge *et al.*, 1992), frog (Carugo *et al.*, 1996) and several bacterial species (Pesce *et al.*, 1997, 2000; Bourne *et al.*,

1996; Forest *et al.*, 2000), and the fold of the enzyme is highly conserved throughout the phyla. The core of the SOD subunit is a flattened Greek-key β-barrel motif consisting of eight antiparallel β-strands joined by three external loops. However, the prokaryotic Cu,Zn SODs are characterized by a distinct quaternary structure from the eukaryotic enzymes, having a different interface region and also being isolated as active and stable monomeric enzymes (Pesce *et al.*, 1997).

The enzyme active site is composed of a Zn^{2+} ion coordinated by three histidines and an aspartic acid (in the human enzyme His63, His71, His80 and Asp83) and by the catalytically active copper. Crystallographic and spectroscopic studies (Bannister *et al.*, 1987; Bertini *et al.*, 1985, 1990; Blackburn *et al.*, 1984; Murphy *et al.*, 1997) demonstrate that the Cu^{2+} and Zn^{2+} ions of oxidized Cu,Zn SODs are bridged by the His63 imidazolate ring. In the oxidized form of Cu,Zn SOD, the copper-coordination geometry is described as distorted square planar, with histidine residues 46, 48, 63 and 120 acting as ligands in the human protein. A water molecule is found about 2.6 Å from the Cu^{2+} ion, weakly coordinating in an axial position relative to the distorted square plane formed by the histidine ligands. On the other hand, in the reduced form of the enzyme the bridging imidazolate is lost as a copper ligand because of protonation of the $N^{\varepsilon 2}$ atom of the bridging His63. Under these conditions, the copper-coordination geometry is nearly trigonal planar, with histidine residues 46, 48 and 120 acting as ligands.

The importance of SOD for species survival is evidenced on the one hand by their strong conservation and on the other by the presence of multiple genes. In humans, for example, three independent genes are located on chromosomes 4, 21 and 6, with the former two coding for cytosolic (SOD1) and extracellular (SOD3) Cu,Zn enzymes and the latter for the mitochondrial Mn enzyme (SOD2). A similar preservation mechanism has also been reported in schistosomes, eukaryotic parasites that are responsible for the debilitating tropical disease known as schistosomiasis, where SOD genes are found on chromosomes 1 and 3. The gene structure of these two forms of Cu,Zn SODs has been well characterized (Simurda *et al.*, 1988; Hong *et al.*, 1992; Mei *et al.*, 1995) and they are known as cytosolic Cu,Zn SOD (SmCtSOD) and signal peptide-containing Cu,Zn SOD (SmSPSOD) or extracellular Cu,Zn SOD owing to the presence of a hydrophobic leader sequence.

Typical characteristics of schistosomal infection include the persistence of adult worms for decades in the host and the deposition of enormous quantities of eggs by female worms. The eggs are usually excreted in the faeces, but occasionally will migrate to dwell in the capillaries of the brain, leading to microinfarction and haemorrhage. The molecular basis of this phenomenon is still unclear, but amongst human parasites appears to be unique to shistosomes. It is possible that SOD plays a significant role in parasite survival within the brain, given the expected free-radical levels generated as a consequence of the elevated oxygen consumption in cerebral tissue.

Furthermore, on infection by *Schistosoma mansoni* the human host mounts an immune response that includes the production of free-radical oxidants by macrophages and leukocytes, which enhances their capacity to kill schistosomes (Callahan *et al.*, 1988). One of the postulated mechanisms by which the parasites counterattack is the production of antioxidants (such as SODs), which act by destroying host-generated free radicals. Location of SmCtSOD and SmSPSOD in the tegument regions might be an adaptive response by the parasite in self-defence against the host immune system, while the location of these enzymes at the gut epithelium might be because the parasite's intestinal lumen is filled with host blood cells, generating an environment for release of reactive oxygen species. These observations have led to speculation that *S. mansoni* SODs may be an indispensable part of an antioxidant protective system for schistosomes (LoVerde, 1998), which suggests that it deserves to be further evaluated in terms of its potential as a target for novel anti-schistosomal therapy.

A homology model for the SmCtSOD structure suggested that two substitutions (E132L and K135V) with respect to the human homologue would be expected to alter the chemical and electrostatic properties of the entrance channel that leads to the active-site copper (Silva, 1999). These observations have stimulated the current study of the crystallographic structure of SmCtSOD as an initial stage in the elaboration of specific inhibitors.

2. Materials and methods

2.1. SmCtSOD structure determination and refinement

The cytosolic Cu,Zn superoxide dismutase from *S. mansoni* (SmCtSOD) was expressed, purified and crystallized and diffraction data were processed as previously described (Cardoso *et al.*, 2001). Briefly, the enzyme was expressed in the form of a GST-SmCTSOD fusion protein in *Escherichia coli* BL21 in the presence of 0.02 m*M* $CuCl_2$ and 0.02 m*M* $ZnCl_2$. The fusion product was subsequently cleaved with human thrombin whilst bound to glutathione Sepharose 4B affinity resin and the soluble product was purified by size-exclusion chromatography on Superdex 75 (both from Amersham Pharmacia Biotech). The enzyme crystallized under identical conditions in both orthorhombic and monoclinic space groups ($P2_12_12_1$ and $P2_1$, respectively; Cardoso *et al.*, 2001). The crystallization conditions, as reported previously, were 0.2 *M* ammonium acetate, 0.1 *M* sodium acetate buffer pH 4.6 and 30% PEG 4000. Of the two crystal forms obtained from PEG 4000, the orthorhombic $P2_12_12_1$ crystals (oSmCtSOD) diffracted to 2.2 Å resolution and the structure was solved by molecular replacement with *AMoRe* (Navaza & Saludjian, 1997) using a homology-built dimeric model of SmCtSOD as a search model. The 1.55 Å monoclinic $P2_1$ structure (mSmCtSOD) was solved by molecular replacement using the 2.2 Å coordinates of oSmCtSOD.

Both SmCtSOD structures were refined using *CNS* (Brünger *et al.*, 1998), employing the maximum-likelihood target function with bulk solvent and anisotropic temperature-factor corrections. Each subunit of the dimer was treated as a rigid body in the initial refinements. The SmCtSOD models

were then refined using torsion-angle simulated annealing. Following these initial stages, the refinement of both models proceeded through cycles of manual rebuilding in *O* (Jones *et al.*, 1991) into σ_A-weighted $2F_o - F_c$, $F_o - F_c$ and $F_o - F_c$ omit maps and positional and temperature-factor refinement. To assess structural accuracy, each of the SmCtSOD subunits was refined independently. A crystallographic R_{free} calculated on the basis of 5% of randomly selected reflections was followed as a monitor of the refinement progress. Topology and parameter files for acetate were obtained from the Hetero-compound Information Center-Uppsala (HIC-Up web server at http://xray.bmc.uu.se/hicup). Water molecules were added automatically using cycles of *ARP* (Collaborative Computational Project, Number 4, 1994) for placement and *CNS* (Brünger *et al.*, 1998) for refinement and then verified by manual inspection in *O* (Jones *et al.*, 1991). Refinement of alternate conformations for several residues and alternate positions for the copper and the copper-coordination water were performed with *REFMAC* (Murshudov *et al.*, 1997), using the maximum-likelihood target function and TLS parameterization, for the mSmCtSOD model. Stereochemical analysis of the refined structures was performed using *PROCHECK* (Laskowski *et al.*, 1993) and *WHATIF* (Vriend & Sander, 1993).

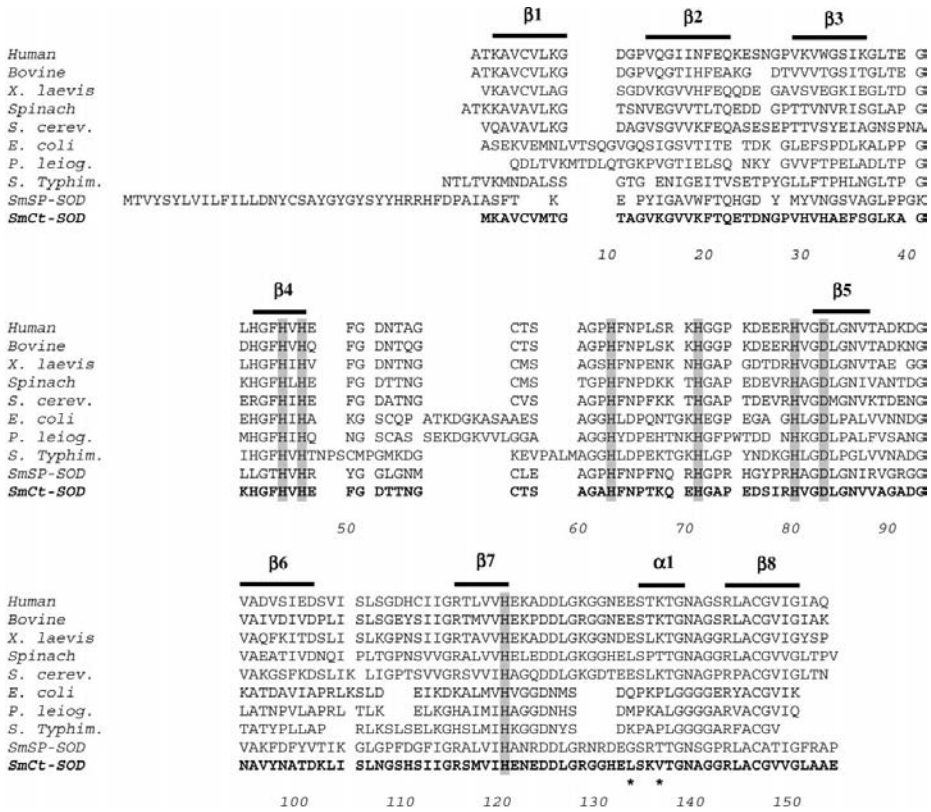

Figure 1
Multiple alignment of Cu,Zn SODs of known three-dimensional structure. Sequences are identified by species name. SmSPSOD refers to the extracellular form of SOD from *S. mansoni* and SmCtSOD to the cytoplasmic form. Secondary-structure elements are identified. Residues whose side chains act as metal ligands are highlighted and the two principal substitutions in the 7,8 (electrostatic) loop observed in *S. mansoni* SODs are indicated with asterisks.

2.2. Structural analysis

Secondary-structure assignment and designation of the disulfide-bridge conformation of SmCtSOD were performed using *PROMOTIF* (Hutchinson & Thornton, 1996). The solvent-accessible surface of the mSmCtSOD structure was calculated using *AREAIMOL* (Collaborative Computational Project, Number 4, 1994), employing a probe radius of 1.6 Å and taking into account crystal packing.

Structural changes between the two structures of SmCtSOD (mSmCtSOD and oSmCtSOD), human Cu,Zn SOD (HSOD) and bovine Cu,Zn SOD (BSOD) were analyzed by least-squares superpositions and visual inspection. Superpositions and root-mean-square deviation (r.m.s.d.) calculations were conducted using the *INSIGHT*II package (Accelrys Inc., San Diego, CA, USA) for all the possible pairwise superpositions of SmCtSOD with HSOD (or BSOD) monomers using only the C^α atoms of the β-strand residues 4–8, 15–20, 29–35, 41–49, 95–100, 113–119 and 144–149 (SmCtSOD sequence numbering).

2.3. Amino-acid sequence alignment

SmCtSOD and SmSPSOD sequences (retrieved from GenBank) were compared with several Cu, Zn SOD sequences using the *MULTALIGN* program from the *AMPS* package in pairwise mode (Barton *et al.*, 1987) with default values. Sequences from Cu,Zn SODs of known three-dimensional structure were used: human SOD (PDB code 1spd), bovine SOD (2sod), *Xenopus laevis* SOD (1xso), *Spinacea oleracea* SOD (1srd), *Saccharomyces cerevisiae* SOD (1jcv), *Escherichia coli* SOD (1eso), *Photobacterium leiognathi* SOD (1yai) and *Salmonella typhimurium* SOD (1eqw). The alignment accuracy was checked by superposition of the C^α coordinates and visualized within the graphics program *O* (Jones *et al.*, 1991).

3. Results and discussion

3.1. Amino-acid sequence variation

The amino-acid sequences of Cu,Zn SODs of known structure were aligned against those of SmCtSOD and

SmSPSOD, respectively, with the former being adopted as a reference for the purposes of sequence numbering in the following discussion (Fig. 1). SmCtSOD has an average sequence identity of 53% with the other eukaryotic Cu,Zn SODs, 25% with the prokaryotic enzymes, 39% with SmSPSOD and 34% with human extracellular SOD3. SmCtSOD is thus sequentially more similar to the human host intracellular enzyme than it is to its own extracellular counterpart. The metal ligands (His45, His47, His62, His70, His79, Asp82 and His119) and the disulfide bridge (between Cys56 and Cys145) are conserved in both SmCtSOD and SmSPSOD. Furthermore, residues responsible for maintenance of the active-site geometry (Gly43, Gly60, Pro65, Gly81, Gly137 and Gly140) and those important for the stability of the Greek-key β-barrel structure (Gly15, Leu37, Phe44, Leu105 and Gly146) of eukaryotic Cu,Zn SODs (Bordo *et al.*, 1994) are conserved in SmCtSOD.

Despite the fact that loops are in general less well conserved across the members of a protein family, in the case of the two SODs from *S. mansoni* the loop between β-strands 7 and 8 responsible for electrostatic guidance is more conserved than some parts of the secondary structure (notably β3 and β6). This is presumably because of its functional role in substrate attraction. However, two important charged residues of this loop, Glu133 and Lys136, in HSOD are replaced by Leu132 and Val135 in SmCtSOD, respectively, and will be discussed in detail below.

3.2. SmCtSOD structural quality

The structures have been solved by molecular replacement and refined in both crystal systems. The SmCtSOD structure in the orthorhombic crystalline form (oSmCtSOD) was refined to a resolution of 2.2 Å, yielding final values of R = 17.6% and $R_{\rm free}$ = 24.1%, whilst the monoclinic structure (mSmCtSOD) was refined to a resolution of 1.55 Å, with R = 15.7% and $R_{\rm free}$ = 17.1%. Simultaneous with the reported R values, both structures present good stereochemistry (Table 1), with 92.6 and 89% of residues falling within the most favoured regions of the Ramachandran plot for mSmCtSOD and oSmSPSOD, respectively. The somewhat larger difference between R and $R_{\rm free}$ for oSmSPSOD may be related to the smaller r.m.s.d. on bond lengths for this structure and is probably a result of the tight restraints applied to the stereochemistry during refinement of this structure as a consequence of the lower resolution in this case.

The oSmCtSOD and mSmCtSOD models consist of two homodimers per asymmetric unit. The two independent dimers are labelled *AB* and *CD*. The electron density for the molecules in the asymmetric unit is clearly defined in both models. There are three additional residues (Gly, Ser and Asn) at the N-terminus of the models as SmCtSOD was expressed as an SmCtSOD-GST fusion protein (Cardoso *et al.*, 2001) and the thrombin-cleavage site is located three residues before the beginning of the SmCtSOD gene. These additional residues are clearly visible in the electron-density maps for all subunits. Besides the polypeptide chain and the active-site metals, the oSmCtSOD structure contains 609 water molecules and one acetate ion hydrogen bonding to Glu22, His29 and a water molecule in one of the four monomers. On the other hand, the mSmCtSOD structure contains 775 water molecules and no acetate. In this structure some residues present alternate conformations, specifically Met1, Ser58, Gln68 and Ser115 in chain *A*, Met1, Thr8, Ser115, Ser133 and Cys145 in chain *B*, Ser58 and Ser115 in chain *C* and Thr8, Ser115 and Cys145 in chain *D*. Furthermore, in mSmCtSOD the electron-density maps showed evidence of disorder in the active-site copper position, which has been modelled as two alternate positions for both the metal and its coordinated water as described below.

We have previously suggested that the two SmCtSOD crystal forms are related by alterations to the crystal packing that leads to an interconversion between crystallographic and non-crystallographic symmetry (Cardoso *et al.*, 2001). This is confirmed by the fully refined structures. The two dimers of the oSmCtSOD structure are related by non-crystallographic translational symmetry, which approximates to half a lattice translation along *a*. On the other hand, the monoclinic cell is approximately half the size along this direction (39.27 Å in mSmCtSOD compared with 74.64 Å in oSmCtSOD),

Table 1
X-ray diffraction data and model statistics for SmCtSOD.

Values in parentheses are for the last resolution shell.

Crystal form	Orthorhombic	Monoclinic
Crystal features		
Space group	$P2_12_12_12$	$P2_1$
No. dimers per AU	2	2
Unit-cell parameters (Å, °)	a = 74.6, b = 78.2, c = 95.2	a = 39.3, b = 95.1, c = 78.4, β = 103.6
Data quality		
X-ray source	Rotating anode	Synchrotron (LNLS)
Wavelength (Å)	1.5418	1.5400
Resolution (Å)	60.00–2.20 (2.27–2.20)	18.00–1.55 (1.59–1.55)
No. observations	114689	325122
No. unique reflections	25229)	80845
Mosaicity (°)	0.28	0.25
Completeness (%)	86.5 (72.9)	99.8 (98.9)
Redundancy	4.5 (3.0)	4.0 (3.6)
$I > 3\sigma(I)$ (%)	81.3 (62.9)	91.2 (74.8)
$R_{\rm sym}$† (%)	8.0 (17.2)	5.1 (12.6)
Structure quality		
$R/R_{\rm free}$‡§ (%)	17.6/24.1	15.7/17.1
No. residues	624	624
No. water molecules	609	775
No. ions	4 Cu^{+}, 4 Zn^{2+}, 1 $C_2H_4O_2^-$	4 Cu^{2+} (2 positions), 4 Zn^{2+}
Average B factor (Å^2)		
Protein overall	13.2	10.2
Cu/Zn/$C_2H_4O_2^-$	15.9/9.8/23.9	10.9/8.6/—
Water molecules	22.9	23.0
R.m.s. deviations from ideality		
Bond lengths (Å)	0.004	0.015
Bond angles (°)	1.3	1.5
Ramachandran plot		
Most favoured region (%)	89.0	92.6
Additional allowed regions (%)	11.0	7.4

† $R_{\rm sym} = \sum_h \sum_i |I_i - \langle I_h\rangle| / \sum_h \sum_i I_i$, where $\langle I_h\rangle$ is the mean intensity for reflection I_h and I_i is the intensity of one observation of the reflection. ‡ $R = \sum_{hkl} |F_o - F_c| / \sum_{hkl} |F_o|$. § $R_{\rm free}$ is R for the data reserved for cross-validation.

suggesting that the non-crystallographic translation in oSmCtSOD is related to a lattice translation in mSmCtSOD. In compensation, the non-crystallographic symmetry relating the two dimers of the monoclinic asymmetric unit is a screw axis which is crystallographic in oSmCtSOD.

3.3. The overall structure

As suggested by the substantial degree of sequence similarity, the typical tertiary and quaternary structures of Cu,Zn SODs are well conserved in SmCtSOD and will be described only briefly here. The two subunits of SmCtSOD are related by an approximate twofold axis along the dimeric interface (Fig. 2). Each subunit folds as a flattened Greek-key β-barrel motif consisting of eight antiparallel β-strands connected by seven loops or turns. Each subunit contains one copper and one zinc ion separated by approximately 6 Å. The active site is located at the base of a shallow channel formed by two loops extending from the β-barrel. In addition to forming the active-site channel, these two loops encode the functional subdomain involved in pre-collision electrostatic guidance of the substrate.

There are no large differences in the overall fold of the oSmCtSOD and mSmCtSOD structures, which have a maximum C^{α} r.m.s. deviation of 0.17 Å and an all-atom r.m.s. deviation ranging from 0.34 to 0.62 Å depending on the individual subunits chosen for the comparison. Both SmCtSOD models show structural asymmetry between the subunits of the dimer. Because oSmCtSOD and mSmCtSOD have a similar crystal packing (Cardoso *et al.*, 2001), this structural asymmetry of the dimer's subunits is likely to be a side effect of the crystal contacts. Nevertheless, the two models of SmCtSOD are very similar. The higher resolution of the mSmCtSOD structure allowed a better characterization of the active-site region than for oSmCtSOD and we will focus on this structure in the following sections.

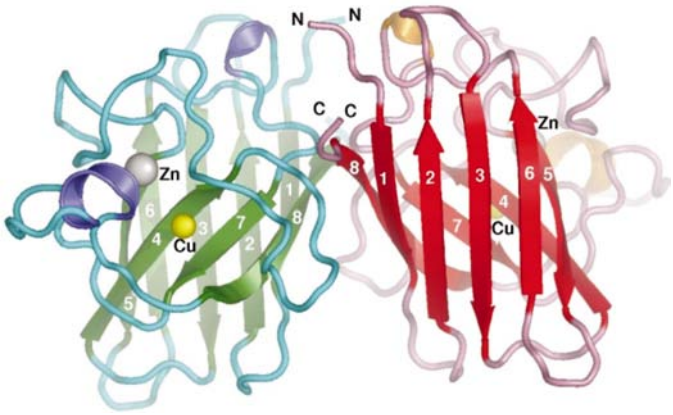

Figure 2
Ribbon representation of the SmCtSOD dimer. Active-site metals are shown as yellow (copper) and grey (zinc) spheres. The β-strands are numbered according to the amino-acid sequence.

3.4. SmCtSOD disulfide bridge

In one of the monomers of each dimer in the asymmetric unit of the mSmCtSOD structure (*B* and *D*) alternate conformations for the disulfide bridge between Cys56 and Cys145 are observed as a consequence of two different rotamers for Cys145 (Fig. 3*a*). One of the disulfide-bridge conformations is a left-handed spiral (which refines to 67% occupancy in chain *B* and 81% occupancy in chain *D*), while the other is a right-handed hook (Richardson, 1981). In fact, an electron-density peak in the $\sigma_A F_o - DF_c$ map (contoured at 5σ) also suggests an alternate conformation for Cys56. However, movement of Cys56 alone is insufficient to fit all atoms within the electron density. On the other hand, there is no density into which to model an alternative conformation for the local backbone. We conclude that the disulfide bridge in the *B* and *D* chains of mSmCtSOD presents significant disorder and may even be broken. The disulfide bridges of the other two monomers (*A* and *C*) of mSmCtSOD and the four subunits of oSmCtSOD show only the left-handed spiral conformation.

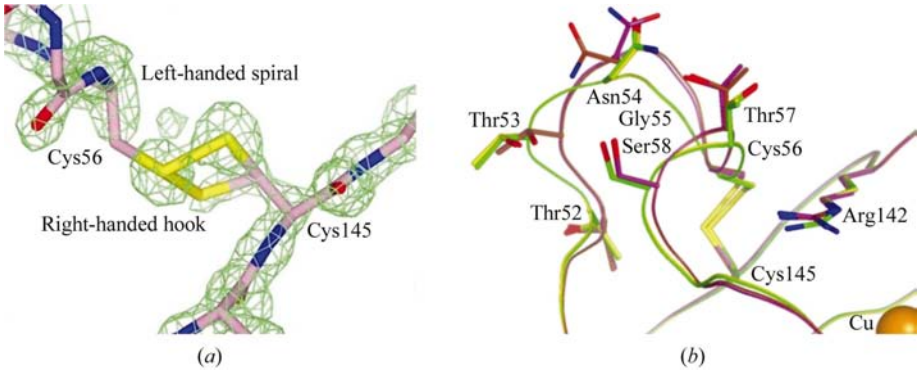

Figure 3
The disordered disulfide-bridge region in mSmCtSOD. (*a*) Disulfide-bridge conformation and electron-density map in the *B* chain of mSmCtSOD. The $\sigma_A F_o - DF_c$ omit map near the disulfide bridge was contoured at 3.0σ (green cage). Alternate conformations (left-handed spiral and right-handed hook) were refined for the disulfide bridge of chains *B* and *D*. (*b*) Movement of the disulfide-bridge subloop in mSmCtSOD. Structural superposition of all four independent subunits in the asymmetric unit of mSmCtSOD (the *A* chain, yellow, and *C* chain, green, are practically indistinguishable; the *B* chain is in brown and the *D* chain purple).

The disordered disulfide bridge of the mSmCtSOD structure may be related to partial photo-reduction during data collection (Burmeister, 2000; Weik *et al.*, 2000). A similar phenomenon has recently been reported for bovine SOD (Hough & Hasnain, 2003). The fact that only one of the monomers in each dimer shows this phenomenon is an indication that these monomers are more susceptible to photo-reduction, presumably owing to crystal packing. However, these monomers are no more solvent-accessible, either globally or locally (in the disulfide-bridge subloop) than subunits which present a unique disulfide-bridge conformation. In fact, subunits *B* and *D* show marginally

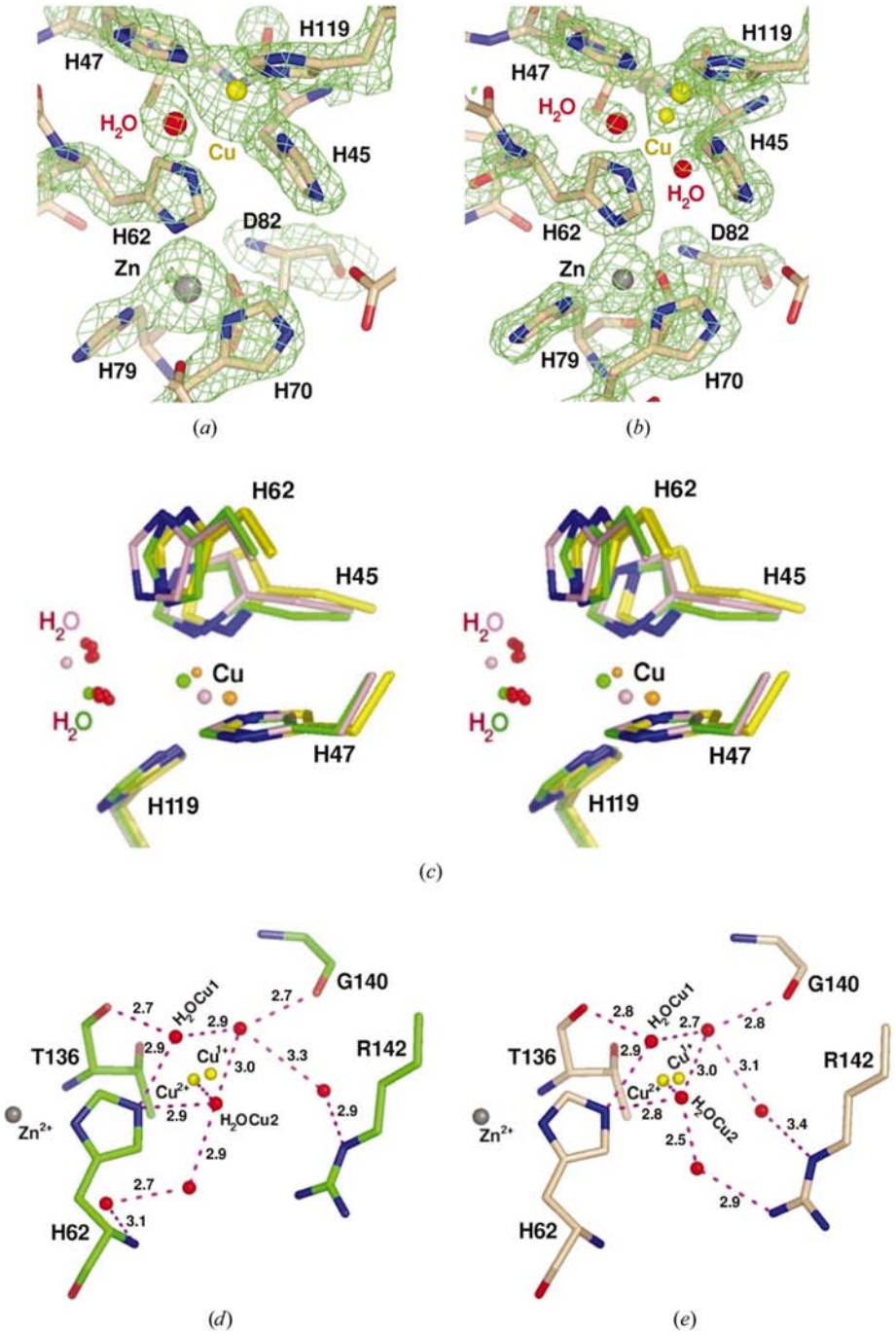

Figure 4
The active site of SmCtSOD. The metals and copper-coordinated water are shown as yellow (copper), grey (zinc) and red (water) spheres. The zinc ion is coordinated by His62, His70, His79 and Asp82. The coordination sphere of copper is dependent on the metal oxidation state. In the active site of oSmCtSOD (*a*), copper is coordinated by His45, His47 and His119. In the active site of mSmCtSOD (*b*), alternate positions were observed for copper (consistent with Cu^{2+} and Cu^{+} states) and the copper-ligand water. σ_A-weighted $F_o - F_c$ omit maps near the active site were contoured at 3.0σ (green cage). (*c*) Stereoview of the superposed active sites of mSmCtSOD and bovine Cu,Zn SOD (BSOD). One of the alternate positions of copper (small orange sphere) in mSmCtSOD (yellow subunits) coincides well with the Cu^{2+} ion (green sphere) of one of the BSOD dimer subunits (green chain), while the other alternate position of copper (large orange sphere) in mSmCtSOD lies close to the Cu^{+} ion (pink sphere) of the other BSOD dimer subunit (pink chain). The copper-ligand water is also presented in two alternate positions in mSmCtSOD (red spheres), which correspond well with the Cu^{2+}-associated water in one BSOD subunit (green sphere) and the Cu^{+}-associated water in the other BSOD subunit (pink sphere). (*d*, *e*) Water network at the active-site region of mSmCtSOD. The water positions related to Cu^{2+} and Cu^{+} are alternate positions of the copper-ligand water in chain *A* (*d*) and chain *B* (*e*) of the mSmCtSOD dimer.

lower total accessible areas than do subunits *A* and *C* when calculated within the crystal context (4754 and 5125 Å^2, respectively, for *B* and *D* compared with 5230 and 5177 Å^2 for *A* and *C*).

The asymmetry in disulfide-bridge disorder may nevertheless still be related to crystal contacts. Unique contacts in mSmCtSOD are associated with an average movement of 0.8 Å for the main-chain atoms of residues Thr52–Ser58 of the disulfide-bridge subloop which includes Cys56 (Fig. 3*b*). These are the largest main-chain differences observed between monomers of the dimer. In the case of chains *A* and *C*, the only crystal contacts in the vicinity of the subloop are made at its entrance. Glu48 and Phe49 of subunits *A* and *C* interact with Lys2 and the C-terminus (Glu153) of symmetry-related *B* and *D* subunits, respectively. In the case of the *B* and *D* chains not only are these interactions different (Glu48 and Phe49 of the *B* and *D* chains interact with Arg127, Gly128 and His130 of chains *A* and *C*, respectively) but a further interaction also exists at the exit to the subloop between Arg127 and Ala61 of *AC*. These differences lead to structural asymmetry between the monomers of the dimer within the crystal, which correlates with disulfide-bridge photo-reduction. However, it is difficult to delineate a causal relationship.

3.5. SmCtSOD active site

Even though SmCtSOD was crystallized under oxidizing conditions, the copper-coordination geometry in all subunits of both structural models is predominantly trigonal planar (Fig. 4). This unusual copper geometry under oxidizing conditions has been reported previously for the Cu,Zn SODs from yeast (Ogihara *et al.*, 1996; Hart *et al.*, 1999), ox (Hough & Hasnain, 1999, 2003) and *S. typhimurium* (Pesce *et al.*, 2000). Moreover, spontaneous reduction of both yeast and bovine Cu,Zn SODs has been observed to occur upon heating (Roe *et al.*, 1988). Therefore, we speculate that X-ray data collection may similarly induce reduction of the

Table 2
Average coordination distances, over the four molecules in the asymmetric unit, in the copper and zinc centres of mSmCtSOD and oSmCtSOD.

In the two last columns, the SmCtSOD models are compared with bovine Cu,Zn SOD (BSOD, PDB code 1cbj, refined using data collected at room temperature; Hough & Hasnain, 1999; BSOD2, PDB code 1q0e, refined using data collected at 100 K; Hough & Hasnain, 2003). Cu^{2+} and Cu^{+} in mSmCtSOD arise from alternate positions of the copper, while Cu^{2+} and Cu^{+} in BSOD belong to different subunits of the dimer. For BSOD2, the distances presented correspond to the *B* subunit. H_2OCu2 is the water position related to Cu^{2+}. H_2OCu1 is the water position related to Cu^{+}.

	mSmCtSOD (Å)	oSmCtSOD (Å)	BSOD (Å)	BSOD2 (Å)
Cu^{2+}—His45 $N^{\delta1}$	1.98 (±0.08)		2.00	2.06
Cu^{2+}—His47 $N^{\varepsilon2}$	2.25 (±0.01)		2.15	2.66
Cu^{2+}—His62 $N^{\varepsilon2}$	2.39 (±0.09)		2.21	2.15
Cu^{2+}—His119 $N^{\varepsilon2}$	2.30 (±0.05)		2.21	2.42
Cu^{2+}—H_2OCu2	2.78 (±0.07)		2.55	2.56
Cu^{2+}—H_2OCu1	2.86 (±0.08)			
Cu^{+}—His45 $N^{\delta1}$	2.04 (±0.01)	2.22 (±0.04)	2.07	2.05
Cu^{+}—His47 $N^{\varepsilon2}$	1.95 (±0.01)	2.08 (±0.08)	1.98	2.01
Cu^{+}—His62 $N^{\varepsilon2}$	3.26 (±0.05)	3.04 (±0.09)	3.20	3.32
Cu^{+}—His119 $N^{\varepsilon2}$	2.02 (±0.02)	2.06 (±0.01)	2.00	2.04
Cu^{+}—H_2OCu2	3.44 (±0.16)	3.30 (±0.07)	3.5	3.69
Cu^{+}—H_2OCu1	3.51 (±0.18)			
Zn^{2+}—His62 $N^{\delta1}$	2.03 (±0.02)	2.06 (±0.02)	1.99	2.05
Zn^{2+}—His70 $N^{\delta1}$	2.04 (±0.01)	2.02 (±0.02)	2.04	2.05
Zn^{2+}—His79 $N^{\delta1}$	2.05 (±0.02)	2.09 (±0.04)	1.92	2.06
Zn^{2+}—Asp82 $O^{\delta1}$	1.90 (±0.04)	1.98 (±0.05)	1.92	2.00
Cu^{2+}—Zn^{2+}	6.01 (±0.04)		6.07	5.97
Cu^{+}—Zn^{2+}	6.69 (±0.02)	6.64 (±0.04)	6.59	6.87
Cu^{2+}—Cu^{+}	0.93 (±0.06)			
H_2OCu2—H_2OCu1	2.31 (±0.28)			

copper in Cu,Zn SODs, since the crystallization conditions and crystal contacts for yeast, bovine and *S. mansoni* Cu,Zn SOD differ too much to be the causal agent of copper reduction. The reduced copper may result from the interaction of the copper with free radical produced by water radiolysis during X-ray exposure (Burmeister, 2000; Weik *et al.*, 2000). An alternative explanation, which cannot be ruled out, is that the enzyme suffers slow reduction in the crystallization medium as has been suggested by Hough *et al.* (2000).

Although the majority of the copper in mSmCtSOD is consistent with Cu^{+}, clearly defined peaks in the $\sigma_A F_o - DF_c$ electron-density map (contoured up to 7σ) near the copper and the copper-ligand water allowed the refinement of a second position for the copper and water in all four chains of the structure (Figs. 4*b* and 5). The dominant position (which we refer to as Cu^{+}) has about ∼85% occupancy. The second position is consistent with a Cu^{2+} geometry. Designation of copper redox states was performed using superpositions between mSmCtSOD and bovine Cu,Zn SOD (PDB code 1cbj) and by reference to the distances between copper and its ligands. The bovine Cu,Zn SOD (BSOD) dimer has one subunit with copper in the five-coordinate oxidized form and the other in the three-coordinate reduced form (Hough & Hasnain, 1999). The low-occupancy copper site in mSmCtSOD superposes well with the copper-oxidized form of

Table 3
Occupancy and *B* factors for the metals and copper-ligand water in mSmCtSOD.

Water molecule occupancies are cited to the nearest 10%. H_2OCu2 is the water position related to Cu^{2+}. H_2OCu1 is the water position related to Cu^{+}.

	Chain *A*	Chain *B*	Chain *C*	Chain *D*
Occupancy (%)				
Cu^{2+}	16	14	16	13
Cu^{+}	84	86	84	87
H_2OCu2	70	30	70	20
H_2OCu1	30	70	30	80
Zn^{2+}	100	100	100	100
B factor (Å^2)				
Cu^{2+}	9.36	9.15	12.63	12.15
Cu^{+}	9.6	9.24	12.49	12.19
H_2OCu2	10.18	11.96	11.86	11.65
H_2OCu1	10.13	11.91	11.76	11.82
Zn^{2+}	7.09	7.84	9.26	10.87

BSOD, while the high-occupancy site superposes well with the copper-reduced form of BSOD (Fig. 4*c*). Furthermore, the distance between the dominant copper position in mSmCtSOD to the $N^{\varepsilon2}$ atom of the bridging His62 is much longer (∼3.2 Å) than that expected for the copper-oxidized form (∼2.3 Å) (Table 2). In addition, the distances between the copper ion and His47, His119 and the zinc ion are sensitive to the copper redox state. The Cu^{+}—Zn^{2+} distance is longer than the Cu^{2+}—Zn^{2+} distance (6.69 and 6.01 Å, respectively) owing to the movement of Cu^{+} away from the zinc into the coordination plane defined by His45, His47 and His119. These values compare well with those reported by Hough & Hasnain (1999).

In a more recent structure of bovine SOD solved to 1.15 Å and refined using data collected at cryogenic temperatures (Hough & Hasnain, 2003), the authors also reported two sites for the copper ion in one of the subunits, with the Cu^{2+} position representing approximately 10% occupancy. Superposition shows that the two copper sites in the bovine struc-

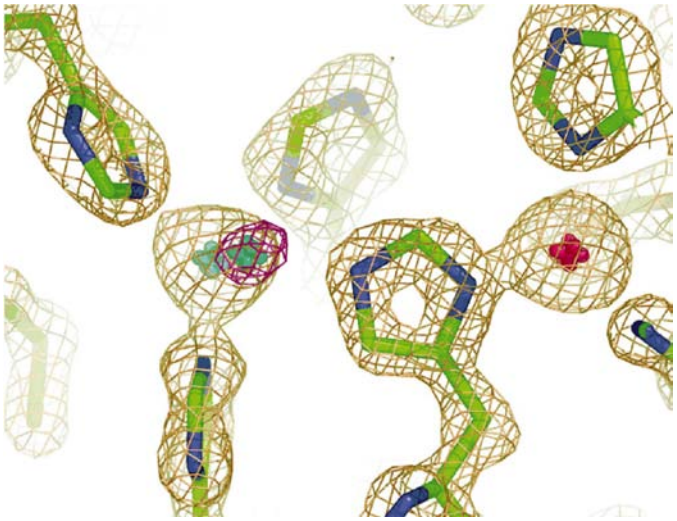

Figure 5
$2F_o - F_c$ (gold) and $F_o - F_c$ (purple) electron-density maps of the active site contoured at 2σ and 5σ, respectively. The zinc ion is shown in red and the two alternative positions for the copper ion are shown in blue.

ture correspond well to those described here for mSmCtSOD. The Cu^{+} to Cu^{2+} vectors lie parallel in both structures, showing that the direction in which the copper moves is identical. However, the average separation between the two sites for the four independent subunits of mSmCtSOD is 0.93 Å (Table 2) compared with a slightly longer distance in the bovine enzyme of 1.36 Å.

The position of the copper-ligand water in the active site of Cu,Zn SODs is also dependent on the redox state of the copper. One of the water positions in mSmCtSOD superposes well with the water in the copper-oxidized form of BSOD, while the other position superposes well with that of the reduced form (Fig. 4*c*). On the other hand, there is an average difference in occupancy of 45% between the equivalent positions of the copper-ligand water from different subunits of the mSmCtSOD dimer (Table 3). In one of the subunits (chains *A* and *C*), the water position related to Cu^{2+} (H_2OCu2) has a higher occupancy (∼70%) than that related to Cu^{+} (H_2OCu1), while the opposite behaviour is observed in the remaining subunit (chains *B* and *D*), where the average H_2OCu2 occupancy is 25%. Although it is difficult to estimate water occupancies with precision, the main message would appear to be that in both pairs of subunits there is a major and a minor water site and that these are different for subunits *A* and *C* compared with *B* and *D*. There is a good correlation between the occupancy of the two copper sites and their associated waters in the case of subunits *B* and *D*, which is not the case for subunits *A* and *C*. In the latter subunits the movement of the water has not fully accompanied the movement of the copper and is indicative of the coexistence of Cu^{+} and H_2OCu2. This may be a reflection of the dynamics of the active site which are necessary for catalysis.

The H_2OCu1 and H_2OCu2 positions are equally stabilized by hydrogen bonds in both subunits of the dimer. H_2OCu1 in both subunits interacts with His62 (which should be protonated under these circumstances), the backbone carbonyl of Thr136 and a water molecule. On the other hand, H_2OCu2 interacts with the metal and two other water molecules, one of which is identical to that described for H_2OCu1 (Fig. 4*d*). The position of the second water varies as a function of the subunit. In the *B* and *D* subunits this water forms a bridge between H_2OCu2 and the side chain of the highly conserved Arg142, which is not the case for subunits *A* and *C*. Arg142 is in turn hydrogen bonded to the backbone of Cys56 which participates in the disulfide bridge described above.

It is of interest to note that the subunit with a higher occupancy for the water related to Cu^{+} (chains *B* and *D*) also has the disordered disulfide bridge, even though the redox state of copper is basically the same in all subunits (Table 3). Therefore, the subunit asymmetry at the active-site region could be related to differential photo-reduction of the SmCtSOD subunits.

Several studies have questioned the involvement of the copper-ligand water in the correct orientation of the substrate, the proton-transference process during catalysis and/or the stabilization of the catalytically important Arg142 (Hart *et al.*, 1999; Hough & Hasnain, 1999; Pesce *et al.*, 1997; Sette *et al.*, 2000). The structure of the Cu,Zn SOD from *E. coli* (PDB code 1eso; Pesce *et al.*, 1997) sheds some light on this discussion, since this enzyme lacks the ligand water molecule without severe consequences for catalytic activity (Pesce *et al.*, 1997; Sette *et al.*, 2000). The *E. coli* enzyme ensures a stable conformation for the Arg142 side chain by a salt bridge found uniquely in this enzyme. In the case of SmCtSOD and bovine

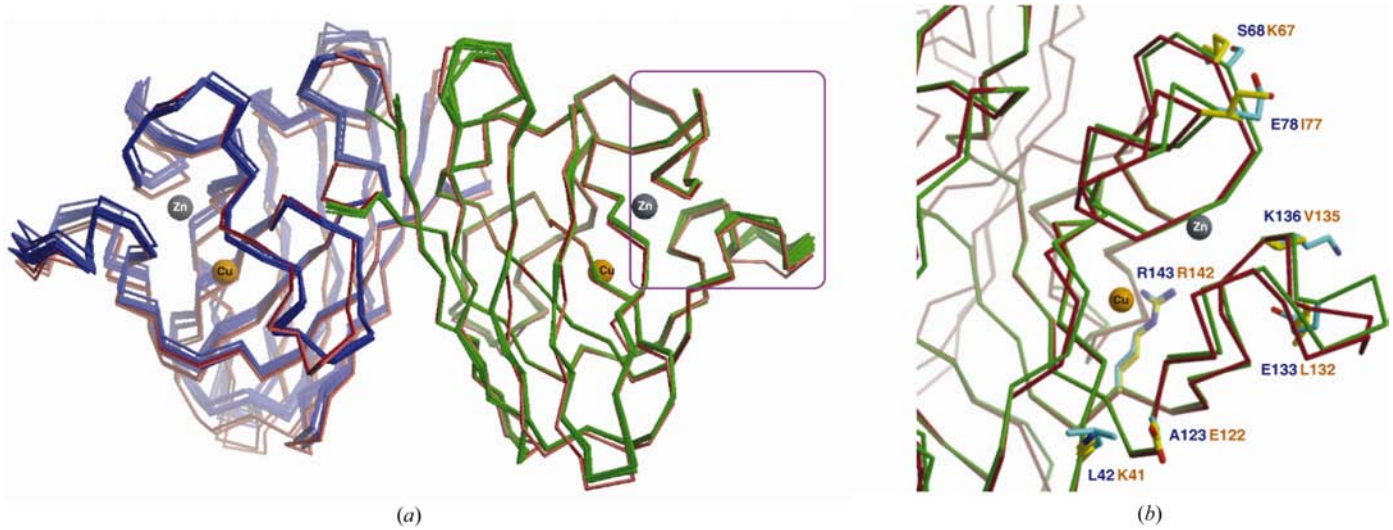

Figure 6
Superposition of the mSmCtSOD and human SOD structures. (*a*) Overall superposition of both dimers of mSmCtSOD in red with the nine crystallographically independent dimers of HSOD in blue/green (PDB code 1hl5; Strange *et al.*, 2003). Only the green subunits of HSOD were used for the superposition on the *A* and *C* chains of mSmCtSOD. The *β*-strand regions of the *A* and *C* chains correspond well to the green chains of HSOD, but the subunits that were not superimposed (on the left of the figure) superpose less well. The active-site region is indicated by the copper (gold sphere) and zinc (grey sphere). The region of the electrostatic loops is indicated by the purple square. (*b*) Superposition of the region of the electrostatic loops in the *A* subunit of both mSmCtSOD (red trace) and HSOD (green trace) with substitutions indicated (yellow side chains in mSmCtSOD and blue side chains in HSOD). Arg142 is conserved in both proteins.

Cu,Zn SOD (Hough & Hasnain, 1999) a hydrogen-bonding network is observed (Fig. 4*d*) with the participation of the copper-ligand water, which could be involved in the stabilization of the Arg142 side-chain conformation.

3.6. SmCtSOD electrostatic loops

There is a small difference in the relative orientations of the two subunits in SmCtSOD compared with HSOD. This is clearly evident in Fig. 6(*a*), in which the *A* and *C* subunits of SmCtSOD (pink and red) have been superposed on one (green) subunit of HSOD. The remaining HSOD subunit (blue) shows a systematic shift with respect to SmCtSOD. There is probably no physiological significance to this finding, which may be the result of crystal-packing forces.

In eukaryotic Cu,Zn SODs, the residues involved in long-range electrostatic substrate guidance and orientation are located principally in the loop between β-strands 7 and 8, one of two large loops which extend from the β-barrel to form the active-site channel (Tainer *et al.*, 1990). Residues at positions 132, 133, 136 and 137 (human sequence numbering) at the rim of the active-site channel determine in many eukaryotic Cu,Zn SODs, together with Arg143, the shape and strength of the electrostatic field around the active site (Getzoff *et al.*, 1983, 1992). Moreover, these four residues compose a hydrogen-bonding network on the solvent-exposed helical turn of the electrostatic 7,8 loop of bovine, human and yeast Cu,Zn SODs (Getzoff *et al.*, 1992).

The 7,8 electrostatic loop of SmCtSOD shows some notable residue substitutions which, however, do not significantly affect its conformation in any of the crystallographically independent SmCtSOD subunits described here. Among these substitutions, the residues Ala123, Glu133 and Lys136 in HSOD are substituted by Glu122, Leu132 and Val135, respectively, in SmCtSOD (Fig. 6). This leads to a local charge difference in the electrostatic loop of -1, with SmCtSOD bearing the more negative charge. There are also a series of substitutions affecting charged residues in the loop between strands 4 and 5. However, these are rather distant from the active-site channel and probably have little impact on substrate guidance. Therefore, although the electrostatic hydrogen-bonding network involving residues at positions 133 and 136 in HSOD is disrupted in the 7,8 loop of SmCtSOD, the electrostatic potential of the loop is only marginally affected, consistent with the comparable catalytic efficiency of the two enzymes (Silva, 1999). This is also consistent with the observations of others (Desideri *et al.*, 1989).

The presence of Leu132 and Val135 within the 7,8 loop leads to the formation of a hydrophobic wall on one side of the channel leading to the active-site copper. Although these two substitutions are not responsible for any overall charge alteration, they may represent a potential opportunity for building specificity into potential SOD inhibitors. The mean distance between the active-site Cu^{2+} site and side-chain atoms of Leu132 and Val135 is approximately 10 Å, suggesting that a typical small-molecule inhibitor or molecule of drug-like proportions would be able to bridge this gap.

3.7. Implications for SmSPSOD

The cytosolic SOD described here is expected to play an important role in the prevention of intracellular oxygen toxicity. On the other hand, it has been suggested that the extracellular enzyme (SmSPSOD) may have a different role, specifically acting as a defence mechanism against attack by the cellular immune system of the host (Simurda *et al.*, 1988). For this reason, the crystal structure of SmSPSOD would be of great interest to parasitologists but has yet to be determined. Nevertheless, some general comments concerning the electrostatic loop of SmSPSOD can be made on the basis of the structure of SmCtSOD.

In SmSPSOD, Leu132 and Val135 of SmCtSOD are substituted by glycine and threonine, respectively. The entrance to the active site is thus less hydrophobic compared with SmCtSOD, but once again does not involve charged residues at these positions as seen in the human enzyme. Furthermore, in SmSPSOD the Gly128–Gly129 sequence of the SmCtSOD electrostatic loop is replaced by Asn–Arg, in which the second glycine, which normally assumes the α_L conformation, is replaced by an arginine. These substitutions would be expected to induce changes in the conformation and charge distribution of the electrostatic loop that may have consequences for substrate encounter and the local topography of the entrance to the active site. It is therefore possible that a potential SOD inhibitor would behave differently with respect to both enzymes and attempts to design such molecules must await a structure determination of SmSPSOD.

This work was supported by grants from the Fundação de Amparo à Pesquisa do Estado de São Paulo (FAPESP), CAPES and PRONEX.

References

Bannister, J. V., Bannister, W. H. & Rotilio, G. (1987). *CRC Crit. Rev. Biochem.* **22**, 111–180.
Barton, G. J. & Sternberg, M. J. E. (1987). *J. Mol. Biol.* **198**, 327–337.
Bertini, I., Banci, L., Piccioli, M. & Luchinat, C. (1990). *Coord. Chem. Ver.* **100**, 67–103.
Bertini, I., Luchinat, C. & Monnanni, R. (1985). *J. Am. Chem. Soc.* **107**, 2178–2179.
Blackburn, N. J., Hasnain, S. S., Binsted, N., Diakun, G. P., Garner, C. D. & Knowles, P. F. (1984). *Biochem. J.* **219**, 985–990.
Bordo, D., Djinovic, K. & Bolognesi, M. (1994). *J. Mol. Biol.* **238**, 366–386.
Bourne, Y., Redford, S. M., Steinman, H. M., Lepock, J. R., Tainer, J. A. & Getzoff, E. D. (1996). *Proc. Natl Acad. Sci. USA*, **93**, 12774–12779.
Brünger, A. T., Adams, P. D., Clore, G. M., DeLano, W. L., Gros, P., Grosse-Kunstleve, R. W., Jiang, J.-S., Kuszewski, J., Nilges, M., Pannu, N. S., Read, R. J., Rice, L. M., Simonson, T. & Warren, G. L. (1998). *Acta Cryst.* D**54**, 905–921.
Burmeister, W. P. (2000). *Acta Cryst.* D**56**, 328–341.
Callahan, H. L., Crouch, R. K. & James, E. R. (1988). *Parasitol. Today*, **4**, 218–225.
Cardoso, R. M. F., Silva, C. H. T. P., Araújo, A. P. U., Tanaka, T., Tanaka, M. & Garratt, R. C. (2001). *Acta Cryst.* D**57**, 1877–1880.

Carugo, K. D., Battistoni, A., Carri, M. T., Polticelli, F., Desideri, A., Rotilio, G., Coda, A., Wilson, K. S. & Bolognesi, M. (1996). *Acta Cryst.* D**52**, 176–188.
Collaborative Computational Project, Number 4 (1994). *Acta Cryst.* D**50**, 760–763.
Desideri, A., Falconi, M., Parisi, V. & Rotilio, G. (1989). *FEBS Lett.* **250**, 45–48.
Djinovic, K., Gatti, G., Coda, A., Antolini, L., Pelosi, G., Desideri, A., Falconi, M., Marmocchi, F., Rotilio, G. & Bolognesi, M. (1992). *J. Mol. Biol.* **225**, 791–809.
Forest, K. T., Langford, P. R., Kroll, J. S. & Getzoff, E. D. (2000). *J. Mol. Biol.* **296**, 145–153.
Fridovich, I. (1986). *Adv. Enzymol. Relat. Areas Mol. Biol.* **58**, 61–97.
Getzoff, E. D., Cabelli, D. E., Fisher, C. L., Parge, H. E., Viezzoli, M. S., Banci, L. & Hallewell, R. A. (1992). *Nature (London)*, **358**, 347–351.
Getzoff, E. D., Tainer, J. A., Weiner, P. K., Kollman, P. A., Richardson, J. S. & Richardson, D. C. (1983). *Nature (London)*, **306**, 287–290.
Hart, P. J., Balbirnie, M. M., Ogihara, N. L., Nersissian, A. M., Weiss, M. S., Valentine, J. S. & Eisenberg, D. (1999). *Biochemistry*, **38**, 2167–2178.
Hong, Z., LoVerde, P. T., Hammarskjold, M.-L. & Rekosh, D. (1992). *Exp. Parasitol.* **75**, 308–322.
Hough, M. A. & Hasnain, S. S. (1999). *J. Mol. Biol.* **287**, 579–592.
Hough, M. A & Hasnain, S. S. (2003). *Structure*, **11**, 937–946.
Hough, M. A., Strange, R. W & Hasnain, S. S. (2000). *J. Mol. Biol.* **304**, 231–241.
Hutchinson, E. G. & Thornton, J. M. (1996). *Protein Sci.* **5**, 212–220.
Jones, T. A., Zou, J.-Y., Cowan, S. W. & Kjeldgaard, M. (1991). *Acta Cryst.* A**47**, 110–119.
Kitagawa, Y., Tanaka, N., Hata, Y., Kusonoki, M., Lee, G., Katsube, Y., Asada, K., Aibara, S. & Morita, Y. (1991). *J. Biochem.* **109**, 447–485.
Laskowski, R. A., MacArthur, M. W., Moss, D. S. & Thornton, J. M. (1993). *J. Appl. Cryst.* **26**, 283–291.
LoVerde, P. T. (1998). *Parasitol. Today*, **14**, 284–289.
Mei, H., Hirai, H., Tanaka, M., Hong, Z., Rekosh, D. & LoVerde, P. (1995). *Exp. Parasitol.* **80**, 250–259.
Murphy, L. M., Strange, R. W. & Hasnain, S. S. (1997). *Structure*, **5**, 371–379.
Murshudov, G. N., Vagin, A. A. & Dodson, E. J. (1997). *Acta Cryst.* D**53**, 240–255.
Navaza, J. & Saludjian, P. (1997). *Methods Enzymol.* **277**, 581–594.
Ogihara, N. L., Parge, H. E., Hart, P. J., Weiss, M. S., Goto, J. J., Crane, B. R., Tsang, J., Slater, K., Roe, J. A., Valentine, J. S., Eisenberg, D. & Tainer, J. A. (1996). *Biochemistry*, **35**, 2316–2321.
Parge, H. E., Hallewell, R. A. & Tainer, J. A. (1992). *Proc. Natl Acad. Sci. USA*, **89**, 6109–6113.
Pesce, A., Battistoni, A., Stroppolo, M. E., Polizio, F., Nardini, M., Kroll, J. S., Langford, P. R., O'Neil, P., Sette, M., Desideri, A. & Bolognesi, M. (2000). *J. Mol. Biol.* **302**, 465–478.
Pesce, A., Capasso, C., Battistoni, A., Folcarelli, S., Rotilio, G., Desideri, A. & Bolognesi, M. (1997). *J. Mol. Biol.* **274**, 408–420.
Richardson, J. S. (1981). *Adv. Protein Chem.* **34**, 167–339.
Roe, J. A., Butler, A., Scholler, D. M., Valentine, J. S., Marky, L. & Breslauer, K. (1988). *Biochemistry*, **27**, 950–958.
Sette, M., Bozzi, M., Battistoni, A., Fasano, M., Paci, M. & Rotilio, G. (2000). *FEBS Lett.* **483**, 21–26.
Silva, C. H. T. P. (1999). PhD thesis, University of São Paulo, Brazil.
Simurda, M. C., Keulen, H. V., Rekosh, D. M. & LoVerde, P. T. (1988). *Exp. Parasitol.* **67**, 73–84.
Strange, R. W., Antonyuk, S., Hough, M. A., Doucette, P., Rodriguez, J., Hart, P. J., Hayward, L. J., Valentine, J. S. & Hasnain, S. S. (2003) *J. Mol. Biol.* **230**, 877–890.
Tainer, J. A., Getzoff, E. D., Beem, K. M., Richardson, J. S. & Richardson, D. C. (1982). *J. Mol. Biol.* **160**, 181–217.
Tainer, J. A., Roberts, V. A., Fisher, C. L., Hallewell, R. A. & Getzoff, E. D. (1990). *A Study of Enzymes II. Mechanism of Enzyme Action*, edited by S. A. Kuby, Vol. II, pp. 499–538. New York: CRC Press.
Vriend, G. & Sander, C. (1993). *J. Appl. Cryst.* **26**, 47–60.
Weik, M., Ravelli, R. B. G., Kryger, G., McSweeney, S., Raves, M. L., Harel, M., Gros, P., Silman, I., Kroon, J. & Sussman, J. L. (2000). *Proc. Natl Acad. Sci. USA*, **97**, 623–628.
Winterbourn, C. C. (1993). *Free Radic. Biol. Med.* **14**, 85–90.